Laminar-turbulent transition prediction for helicopter rotors in hover and forward flight – a RANS based investigation of transition mechanisms using empirical criteria

C. C. Heister
German Aerospace Center (DLR)

Institute of Aerodynamics and Flow Technology, Helicopter,
Lilienthalplatz 7, D-38108 Braunschweig, Germany

E-mail: christoph.heister@dlr.de

ABSTRACT

The present paper deals with the laminar-turbulent transition prediction on helicopter rotors in hover and forward flight for RANS based rotor performance prediction. The investigation employs empirical criteria and covers transition mechanisms due to Tollmien-Schlichting and crossflow instabilities, laminar separation, bypass transition and attachment line contamination. An integral method and a family of chord- and spanwise velocity profiles are used for an approximate calculation of the laminar boundary layer quantities. The predicted transition positions are compared to the experimental data of a BO 105 in hover (DLR flight test) and of the 7AD rotor in forward flight (GOAHEAD wind tunnel test). The effect of the laminar flow on the predicted rotor performance is studied by comparison to fully turbulent results.

SYMBOLS

Symbol	Units	Explanation
Latin symbols		
c	m	chord length
c_P	-	power coefficient
c_T	-	thrust coefficient
FM	-	figure of merit $FM = c_T^{3/2} / \left(\sqrt{2} \cdot c_P\right)$
H_{12}	-	form factor
k	m^2/s^2	specific turb. kinetic energy
M	-	Mach number
r	m	radius
R	m	rotor radius
Re	-	Reynolds number
$Re_{\delta 1}$	-	displacement thickness Re
$Re_{\delta 1,CF}$	-	crossflow displ. thickn. Re
$Re_{\delta 2}$	-	momentum thickness Re
s	m	arc length
Tu	-	turbulence level
U	m/s	chordwise BL edge velocity
$U_{\parallel}$	m/s	incident flow parallel to AL
$U_{\perp}$	m/s	incident flow normal to AL
U_e	m/s	velocity at BL edge
W	m/s	radial BL edge velocity
x/c	-	relative chord length
Greek symbols		
δ_1	m	displacement thickness
δ_2	m	momentum thickness
ε_τ	-	wall shear stress ratio
Θ	°	collective pitch
Λ	°	yaw angle
μ	-	advance ratio
Ψ	°	rotor azimuth angle
Subscripts		
C		chord direction
T		transition onset

Abbreviation	Explanation
AHD	Arnal, Habiballah & Delcourt
AL(T)	attachment line (transition)
BL	boundary layer
BVI	blade vortex interaction
Byp	bypass (transition)
CF	crossflow (transition)
LE	leading edge
LS	laminar separation
(U)RANS	(unsteady) Reynolds averaged Navier-Stokes equations
RF	reverse flow
TE	trailing edge
TOW	take off weight
TS	Tollmien-Schlichting
Tu	(incident flow) turbulence

1. INTRODUCTION

Within the rotorcraft industry, RANS methods have gained more and more importance during the last years, seeing intensified application during the design and development phase of advanced helicopter technologies. Looking at the design phase of new rotors, an evolving application area for RANS methods is the

accurate prediction of flight performance data [6]. In the context of performance prediction, the state of the boundary layer flow significantly influences the amount of skin friction on the blade surface, with considerably lower values in the laminar than in the turbulent flow areas. Thus, a capability to predict the laminar-turbulent flow state during RANS computations is one of the key components of an accurate helicopter performance calculation. Generally, the stability of the laminar boundary layer and its transition to turbulent state are affected by various flow parameters like e.g. the Mach and Reynolds number (Re), the freestream turbulence level (Tu), the characteristic of the pressure gradients or the occurence of radial (spanwise) velocity components [1]. Since helicopter rotors typically operate in a complex flow field [11], large variations of the transition-relevant flow-parameters result from the vortices trailing at the blade tips and the superposition of the rotary/translatory blade motions. Flow phenomena like yawed/reversed flow, compressibility effects or blade-vortex interaction (BVI) may occur and potentially lead to different instability mechanisms. Previous publications have studied transition on hovering rotors with respect to Tollmien-Schlichting (TS) (see e.g. [10], [8] and [9]) or TS / crossflow (CF) instabilities [5]. For rotors in forward flight, occasional publications have dealt with the numerical prediction of TS instabilities [21] and TS/CF instabilities [3]. In the latter paper, laminar-turbulent rotor calculations were performed with respect to drag prediction. The present work numerically investigates the occurrence of multiple transition mechanisms at hover and forward flight and their influence on rotor power. Among the considered mechanisms are TS and CF instabilities, laminar separation (LS), bypass (Byp) instabilities and attachment line transition (ALT). With respect to industrial application, emphasis is laid on a robust, fast and sufficiently accurate calculation of the required boundary layer (BL) data, obtainable from RANS meshes with a standard resolution of approximately 24 points inside the BL.

2. FLOW SOLVER

The block-structured flow solver FLOWer [14] of DLR is used for the present investigations. It solves the compressible three-dimensional Reynolds-averaged Navier-Stokes equations for rigid or deforming bodies in arbitrary motion. A finite-volume method with second order central space discretization including scalar or matrix dissipation is used. The cell-centred formulation for space discretization is employed. A multistage Runge-Kutta scheme explicitly integrates the discrete equations. For unsteady computations the Dual-Time-Stepping approach is used. To accelerate convergence, several techniques, including local time stepping, implicit residual smoothing and multigrid are available. Complex geometries and independently moving bodies can be flexibly handeled with the Chimera technique. Various turbulence models are available, ranging from eddy viscosity to full differential Reynolds-stress models.

3. TRANSITION PREDICTION ALGORITHM

The transition prediction algorithm is directly implemented into the flow solver FLOWer and uses the computed RANS data of the BL flow. The prediction algorithm is suited to handle airfoil or wing like geometries. It operates along the grid lines of airfoil sections, as schematically shown in Figure 1.

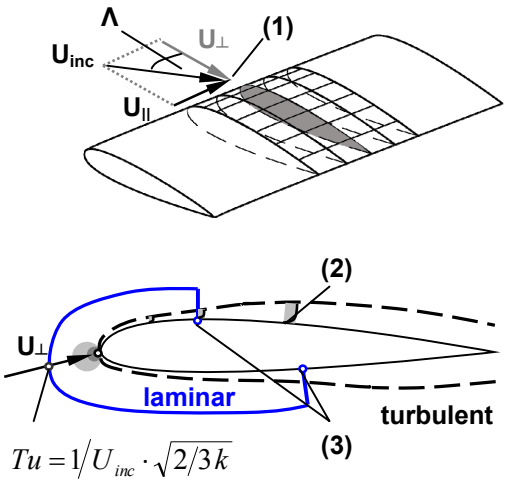

Figure 1: FLOWer transition prediction algorithm (schematic) – top: determination of incident flow conditions; bottom: initialization of laminar zone suppressing production of eddy viscosity.

Upon user preset intervals of the RANS solver iterations, three basic steps are executed: (1) the determination of the incident flow conditions, (2) the calculation of approximated BL data and (3) the prediction of transition onset by empirical criteria. Based on the predicted transition onset position, a laminar flow zone is initialized by blanking the turbulence production term of the active turbulence model. The laminar zone extends from the wall surface into the flow field. Its height is user specified by a number of grid points. For helicopter rotors in forward flight, areas of reverse flow may exist on the retreating side of the rotor disk. If the stagnation point is detected outside a preset tolerance at the leading edge (LE), reverse flow is assumed. In this case, the calculation of the BL data (2) and the prediction of transition (3) will be skipped. The flow is then assumed to be fully turbulent due to the ill defined flow conditions at the airfoil under reverse flow.

3.1 Determination of incident flow conditions

The required incident flow conditions at an airfoil section consist of the velocity components normal ($U_\perp$) and parallel ($U_{||}$) to the attachment line as well as the turbulence level (Tu). The magnitude of the normal flow $U_\perp$ is derived from the stagnation point pressure using the compressible Bernoulli equation. The orientation and magnitude of $U_{||}$ is determined by projecting the incident velocity U_{inc} vector onto the attachment line (see Figure 1, top). The Tu level can be determined at each radial section based on the turbulent kinetic energy upstream of the stagnation point (see Figure 1, bottom). This option is intended for flow cases with a spatial and temporal variation of the Tu level, as for example in the wake/vortex dominated flow fields of helicopter rotors. Alternatively, for known inflow conditions, the Tu level can be prescribed as a constant critical n-factor in the flow field, converted via the Mack relation [1]. The critical n-factor represents the amplification ratio of the most amplified TS wave causing a breakdown to turbulence.

3.2 Approximation of laminar boundary-layer data

The calculation of laminar BL quantities by integrating RANS velocity profiles usually requires a fine grid resolution near the wall (60 points and more). To reduce the required amount of grid points for laminar-turbulent calculations, an integral method according to Schlichting is used [16]. This approximate method is based on a one-parametric set of Hartee velocity profiles. It describes the incompressible state of the BL quantities, namely the displacement and momentum thickness (δ_1, δ_2) as well as the form factor (H_{12}). A compressibility correction of the BL quantities based on the BL edge Mach number [20] is further available in FLOWer. The computation of the BL quantities is done along grid lines of a static or moving mesh. The required BL edge velocity is derived from the compressible Bernoulli equation using the incident velocity and the pressure distribution at the wall (see Figure 2).

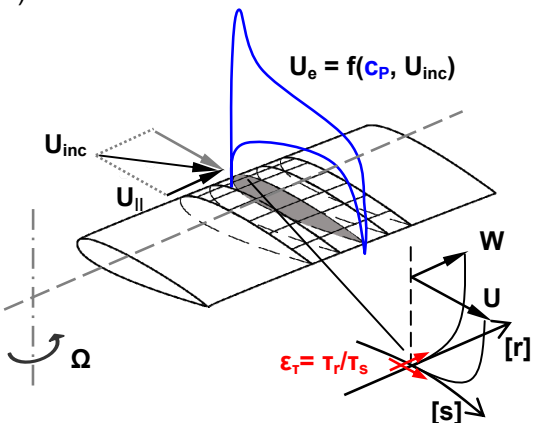

Figure 2: Schematic of the RANS parameters, relevant for the calculation of the laminar BL quantities for the integral method [16]) and the laminar velocity profiles on rotating blades [20].

The pressure normal to the wall is assumed constant within the BL. For 3D flow cases, the streamwise BL quantities (δ_1, δ_2, H_{12}) of the blade are calculated according to the assumptions of an infinite swept wing [7]. At the BL edge, $U_{||}$ is assumed constant in chordwise direction. The calculation of the crossflow Reynolds number ($Re_{\delta 1,CF}$) is based on the integration of a set of velocity profiles for rotary

wings, as developed by Blaser and Velkoff [4]. These velocity profiles have been derived from the three-dimensional momentum-integral equations, respecting coriolis and centrifugal forces. The shape parameters generating the velocity profiles depend on the local wall shear stress ratio in radial/chordwise direction (ε_T), on the BL edge velocities (U, W) and their gradients (dU/ds, dU/dr, dW/ds, dW/dr) (see Figure 2).

3.3 Transition prediction by empirical criteria

The complex flow field of helicopter rotors potentially favours a spectrum of different transition mechanisms. Decelerated flow along the airfoil contour potentially causes TS instabilites and LS. High local yaw angles, as encountered at the rotor blades during forward flight, result in yawed flow causing crossflow components in the BL. Wake and vortex systems induced by the rotor blades represent instabilitiy sources which can bypass the linear TS mechanisms. Considering the combination of local yaw angles and turbulent wakes, the attachment line at rotor blades may be contaminated by turbulent flow, prohibiting any further laminar flow. Based on these considerations a set of empirical transition criteria has been implemented into the FLOWer code in order to study TS/LS, CF, Byp and AL instabilities. The mechanism leading to the most upstream transition onset defines the effective transition onset position. Since some of the considered mechanisms, like Byp, can only be characterized by empirical relations, this study concentrates on the general use of empirical criteria for the sake of consistency. Each individual mechanism is represented by a single criterion. Thus a clear indentification of the relevant transition mechanisms is possible within this study. The chosen approach assumes, that there is no interaction between the individual transition mechansims (independence principle).

3.3.1 Tollmien-Schlichting instabilities and laminar separation

For transition prediction due to longitudinal Tollmien-Schlichting waves, the AHD criterion [1] is used. The AHD criterion is valid for attached flows. It considers the history effects of the pressure gradient, the stability properties of the BL flow and the destabilizing influence of the Tu level. The occurrence of LS is detected during the computation of the laminar BL quantities. If the form factor of the Hartee profiles reaches a value relating to zero wall shear stress [20], then transition due to LS is assumed at the corresponding position.

3.3.2 Crossflow instabilities

To predict crossflow instabilities, the C1 criterion proposed by Arnal [1] is used. It is based on an empirical correlation of the streamwise shape factor H_{12} and the CF Reynolds number ($Re_{\delta 1,CF}$) at the location of transition onset. The present implementation respects the restriction of the criterion to accelerated flows near the LE, with streamwise form factors lower than 2.7. A compressibility correction based on the BL edge Mach number, given in [2], is available in FLOWer.

3.3.3 Bypass instabilities

The Mayle criterion [12] is used to predict bypass transition, triggered by wakes of different Tu intensity. The criterion correlates the momentum thickness Reynolds number at transition onset to the Tu level of the incident flow. Good correlation to experimental data for both adverse and favourable pressure gradients is given for Tu > 3%. The criterion sees frequent use in the design of gas turbine engines.

3.3.4 Attachment line contamination

Laminar flow at an airfoil section may be prohibited due to a turbulent BL at the AL [1]. The fully turbulent state can either be caused by natural transition of the flow along the AL or by a contamination with incident turbulent flow. The momentum thickness Reynolds number of the AL ($Re_{\delta 2,AL}$) can be calculated based on $U_{||}$ and the flow gradient dU_e/ds at the stagnation point. Critical values of $Re_{\delta 2,AL}$ have been experimentally determined to indicate contamination ($Re_{\delta 2,AL}>100$) [13] or natural transition.

3.4 Modelling of the transition length

The length of the transition region from laminar to turbulent state can be defined by the user in terms of grid points downstream of a predicted transition onset. For all presented investigations, a length of one grid point has been found to result in overall stable convergence behaviour. This approach has been chosen with respect to practical application, rather than for a physical modelling of intermittency. For strong adverse pressure gradients, as occurring in the presented flow cases, the intermittency phenomenon has been experimentally found to be no more involved in the transition process [1].

4. SOMERS AIRFOIL NLF-0416

For a basic validation of the presented transition prediction method, a steady 2D testcase is computed, consisting of the natural laminar flow airfoil NLF(1)-0416 [19].

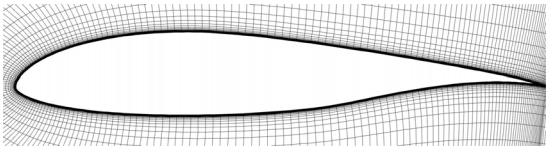

Figure 3: Somers airfoil – structured C-mesh with 337x72 points (close up).

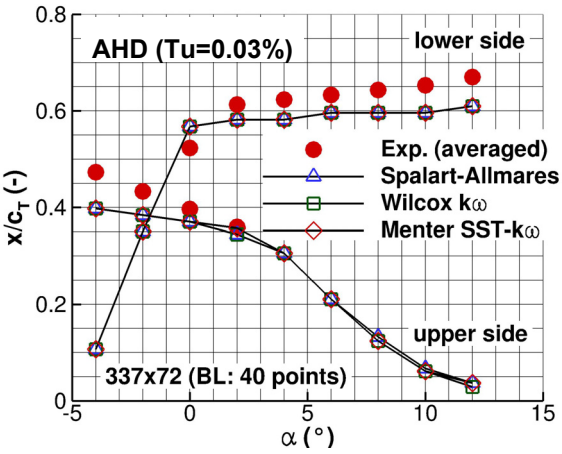

Figure 4: Somers airfoil – comparison of experimental and predicted transition onset positions (M=0.1, Re=4.0 Mio.).

The computational flow conditions correspond to a low Mach number flow at *M=0.1* and a Reynolds number of $Re=4.0 \cdot 10^6$. The Tu level is set to 0.03%. Angles of attack vary in the range from -4° to +12°. The FLOWer computations are performed on a single block C-mesh with *337x72* points, as shown in Figure 3, with a resolution of the boundary layer of approximately 40 points ($y^+<0.5$). The Spalart-Allmares, Wilcox kω and Menter SST-kω turbulence models are used to study possible influences on the transition prediction behaviour. Transition positions are predicted due to TS/LS instabilities, as presented in Figure 4. The match to the averaged experimental data is close, with a general upstream trend. The upstream trend to the experimental data is based on the prediction of LS, as detected during the calculation of the attached laminar BL data (see chapter 3.3.1). For the computed range of angles of attack, the prediction accuracy shows no sensitivity to the choice of investigated turbulence models.

5. BO 105 IN HOVER

To study the transition mechanisms for a helicopter rotor in hover, an isolated main rotor of a BO 105 helicopter is simulated. The computational case refers to a flight test conducted at DLR [15]. During the flight experiment, one of the four main rotor blades was painted with Acenaphthene in order to visualize regions of laminar flow (see Figure 5). It was found that laminar areas extend to approximately 25% chord length on the upper and 70% chord on the lower side. The blade features a NACA 23012mod airfoil and has a radius of 4.92m with -8° linear twist. The hover conditions are set to $M_{TIP}=0.64$ and $Re_{TIP}=4.03$ million at ISA/NN for a steady FLOWer computation. The grid (see Figure 6) uses the chimera technique, consisting of a background grid (approximately 1.72 million points) and an embedded child grid for the blade (1.44 million points). The blade rotates counter clockwise. Periodic, slip wall and Froude boundary conditions are set at the background grid boundaries. The blade surface is resolved with 141 points in chordwise and 97 points in radial direction. Approximately 20 points resolve the BL. The rotor precone angle is 2.5°. A rigid blade structure is assumed. The collective pitch setting matches a TOW of 2250kg ($c_T=0.0050$, $\theta_{r/R=0.7}=5.3°$). The laminar-turbulent computations are started from a fully turbulent solution with

converged thrust and power coefficients. For turbulence modelling, the Wilcox kω model is used. The transition prediction algorithm is called every 50 solver iterations.

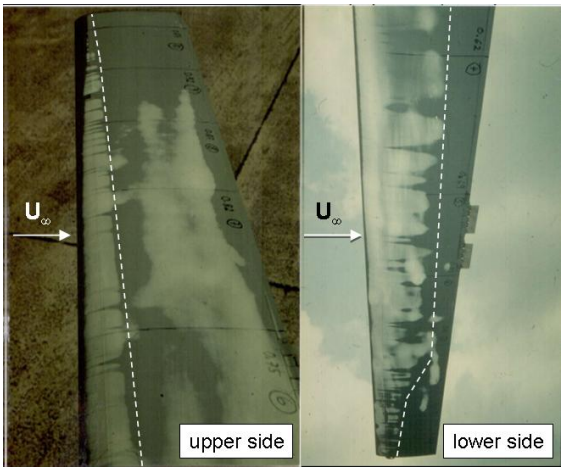

Figure 5: BO 105 hover flight test – photos of Acenaphthen coated blade; light areas indicate areas of laminar flow (schematically indicated by dotted line) [15].

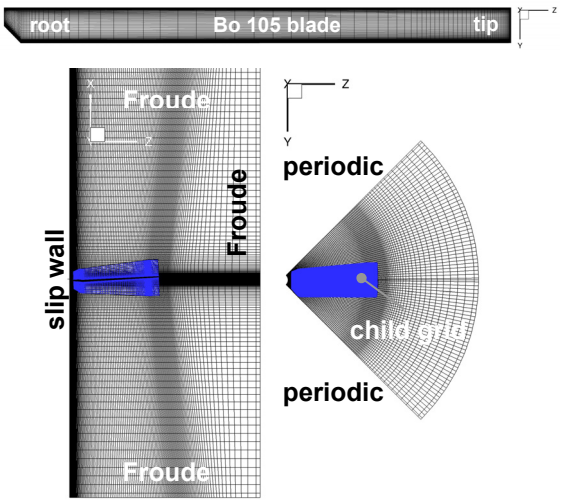

Figure 6: Isolated BO 105 rotor at hover – surface grid (top) and chimera grid topology (bottom) with associated boundary conditions.

5.1 Tollmien-Schlichting transition with prescribed and detected Tu levels

At hover, the main rotor operates in it's own wake. Vortices are shed at the tip and root of the rotor blade and lead to interaction with the trailing blade. Figure 7 illustrates the vortex trajectories of the present hover simulation. The vortices are propagated through the computational domain and lead to BVIs in the root and tip area. A corresponding increase of the incident Tu level can be observed at the tip and root region of the blade (see Figure 8, top).

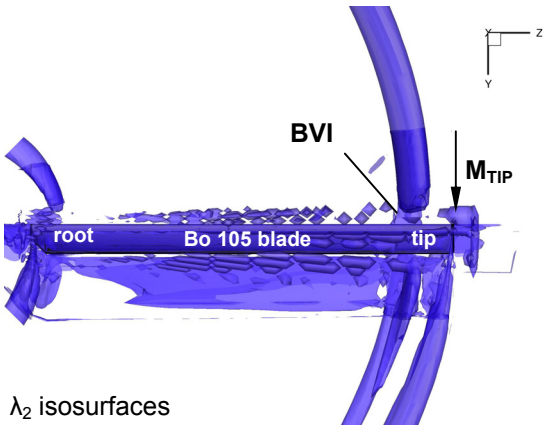

Figure 7: Isolated BO 105 rotor at hover (top view) – rotor wake system (RANS computation, M_{TIP}=0.64, Re_{TIP}=4.03 million).

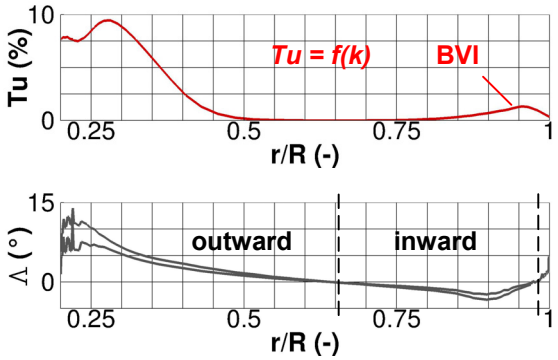

Figure 8: BO 105 rotor in hover – RANS based Tu level and incident flow orientation at the blade leading edge (M_{TIP}=0.64, Re_{TIP}=4.03 million).

With respect to transition prediction, the difference between the use of a constant Tu level (corresponding to n_{CRIT}=6) and the detected incident Tu level can be studied in Figure 9. On the lower side near the tip, the locally detected Tu level leads to an upstream shift of the transition onset, indicating the impact of the vortex. The resulting transition line (solid line) shows an improved match to the flight test data, while the assumption of a constant Tu level (dashed line) indicates transition further downstream of the experimental data. On the

upper side of the blade tip area, the strong flow acceleration within the suction region overrules the potential BL destabilization of the local Tu level. The overall match of the predicted transition onset to the experimental data is close, on both upper and lower side. The physical nature of the high Tu level near the root has to be treated carefully. It probably results from a slowly decaying interaction of the root vortex / rotor inflow as well as an unphysical wake expansion due to numerical discretization errors. Since the method of local Tu detection leads to an overall closer representation of the experimental transition onset, especially in the aerodynamically effective parts of the blade (r/R>0.7), it will be used throughout the following investigations.

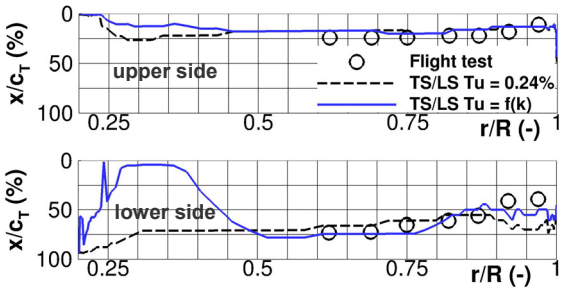

Figure 9: BO 105 rotor in hover – comparison of experimental and predicted transition positions (M_{TIP}=0.64, Re_{TIP}=4.03 million).

5.2 Effective transition of multiple instability mechanisms

Figure 10 presents the predicted laminar flow areas on the blade, considering transition mechanisms due to TS/LS, CF, Byp, and AL instabilities. For comparison, the graph includes the predicted onset positions considering only the TS/LS instabilities (*Tu=f(k)*). The main differences between both numerical results can be observed in the vicinity of the root and tip area. For the major part of the upper side, transition occurs due to TS/LS transition at approximately 18% chord length, triggered by the adverse gradients of the airfoil pressure distribution. Near the root and tip, Byp transition sets in due to the high Tu levels associated to the BVI (compare Figure 8). At the very end of the tip, 3D effects lead to CF transition near the LE, on both upper and lower side. In comparison with the experimental data, the general trend of the predicted laminar areas also matches well to the flight test data on the lower side. Transition at the middle part of the blade is predicted at approximately 75% chord length due to TS/LS (see Figure 10). Towards the tip, a large area of Byp transition continuously shortens the laminar running lengths to 15% chord length. The root and inner part of the blade are affected by CF transition. The occurrence of CF instabilites can be related to the presence of the outward incident flow (compare yaw angle $\Lambda=arctan(U_{||}/U_{\perp})$ in Figure 8). The AL was not contaminated at any part of the blade for all laminar-turbulent computations.

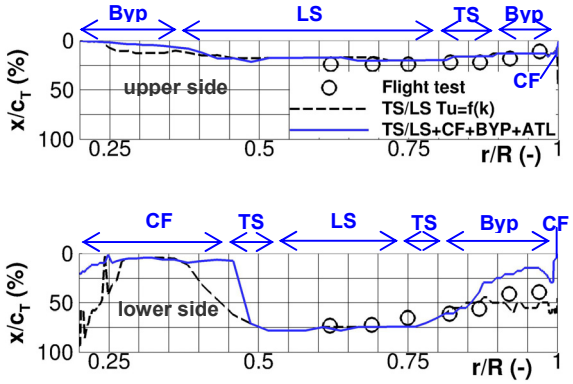

Figure 10: BO 105 rotor in hover – comparison of experimental and predicted transition positions (M_{TIP}=0.64, Re_{TIP}=4.03 million).

5.3 Influence of laminar flow on required rotor power

The influence of the predicted laminar flow on the rotor performance is illustrated in Figure 11. The presented coefficients for thrust (c_T), power (c_P) and figure of merit (FM) of the laminar-turbulent calculations are normalized using the corresponding fully turbulent value. The general increase of the FM for the laminar-turbulent calculations relates to the low skin friction of the laminar flow areas. The power coefficients are reduced by -6% (TS/LS, *Tu=0.24%*) to -4% (TS/LS+CF+BYP+ALT). The thrust coefficient c_T remains practically unaffected and is equal to the fully turbulent value. In consequence, the figure of merit differs to the fully turbulent value in the range of +6% (only TS/LS, *Tu=0.24%*) to +4%

(TS/LS+CF+BYP+ALT). The difference of 2% between the laminar-turbulent calculations mainly relates to the BVI induced Byp transition at the lower blade tip (compare Figure 10).

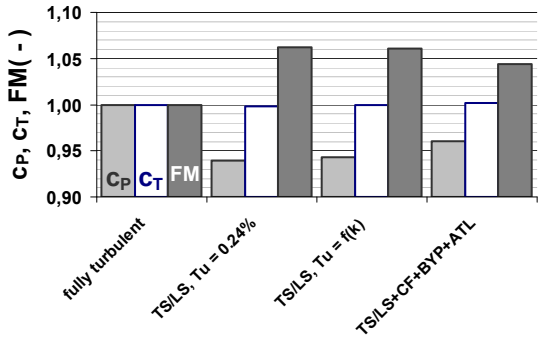

Figure 11: BO 105 rotor in hover – comparison of predicted rotor efficiency for laminar-turbulent calculations (values related to fully turbulent results, M_{TIP}=0.64, Re_{TIP}=4.03 million).

6. 7AD ROTOR IN FORWARD FLIGHT

To investigate the transition mechanisms for a rotor in forward flight, a test case from the GOAHEAD wind tunnel campaign [17] is selected. During the campaign, the four bladed 7AD main rotor of the GOAHEAD test configuration was equipped with hot films at selected radial stations. Thus a comparison between the computed and experimentally determined transition onset positions is possible. The computational test case consists of the isolated 7AD rotor at cruise condition (GOAHEAD TC3-4, advance ratio μ=0.33, shaft angle=-7.5°, clockwise rotation) with a freestream Mach number of M=0.204 and a rotor tip Reynolds number of Re_{TIP}=0.86 million. The resulting chord based Reynolds number distribution over the rotor disk is shown in Figure 14. The blade control angles for the pitch, flap and lag motions of the blades are prescribed as rigid body motions and correspond to the experiment. The blade structure is assumed rigid. A structured chimera grid with a total of 6.49 million points represents the forward flight state of the isolated rotor (see Figure 12). The background grid consists of 3.05 million points, with prescribed farfield and slip wall boundary conditions to represent the DNW-LLF wind tunnel setup in the closed test section. One blade grid consists of 0.86 million points. The blade surface is resolved with 149 points in chordwise and 61 points in radial direction. The boundary layer is resolved with approximately 20 points.

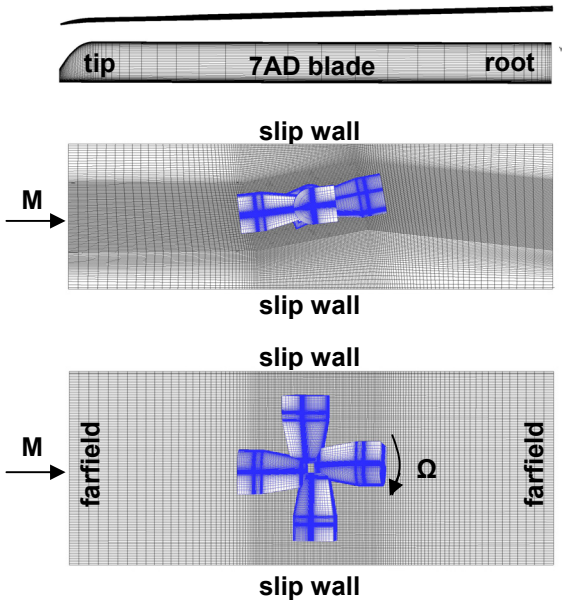

Figure 12: Isolated 7AD rotor in forward flight - surface grid and chimera grid topology with farfield and no-/slip wall boundary conditions (side and top view).

As first step, fully turbulent flow is assumed and the simulation is run for three rotor revolutions in order to assure a fully developed and periodic rotor flow field, using the Wilcox kω turbulence model. The physical time step during the computation corresponds to 1° rotor azimuth. Figure 13 shows the resulting wake structure. Based on the fully turbulent flow solution, a computation with activated transition prediction for one additional rotor revolution is started. The transition prediction algorithm is called twice within the 70 inner iterations of the Dual-Time-Stepping scheme. As in the hover case (see chapter 5), a spectrum of transition mechanisms including TS-instabilities, CF, Byp and AL contamination ($Re_{\delta 2,CRIT}$=100) is investigated. The Tu level of the incident flow at the blades is detected locally. The laminar BL quantities are corrected by the Walz compressibility correction. At first, the behaviour of the individual transition mechanisms will be analyzed. In a second step, the effect of the resulting laminar running length on the required rotor power is investigated.

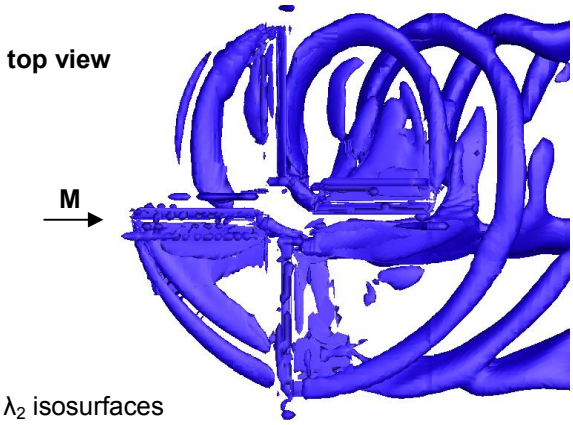

Figure 13: Isolated 7AD rotor in forward flight – rotor vortex trajectories (URANS computation, μ=0.33).

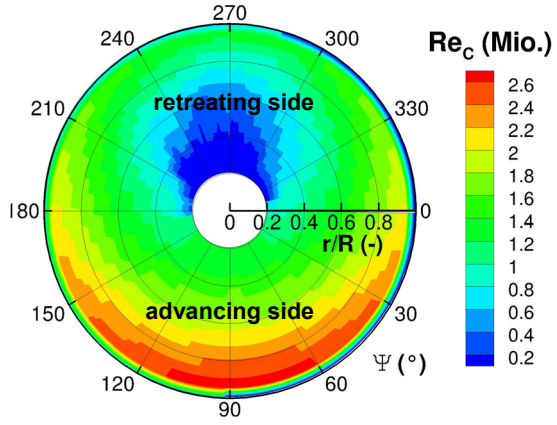

Figure 14: 7AD rotor in forward flight – chord based Re over the rotor disk (μ=0.33, M=0.2, Re_{TIP}=0.86).

6.1 Tollmien-Schlichting transition

Figure 15 shows the transition onset positions as predicted due to pure TS/LS-instabilities during one revolution. For the major part of the revolution, laminar flow exists over 20% chord length on the upper and 80% on the lower side. The TS/LS mechanism closely relates to the commanded blade pitch position and the resulting pressure distribution of the airfoil. Low blade pitch Θ (see Figure 16, *Ψ=[60°; 150°]*) results in low or slightly negative angles of attack, as encountered on the advancing side of the rotor. This favours laminar flow on the upper side and shortens laminar areas on the lower side (compare Figure 15, *Ψ=[60°; 180°]*).

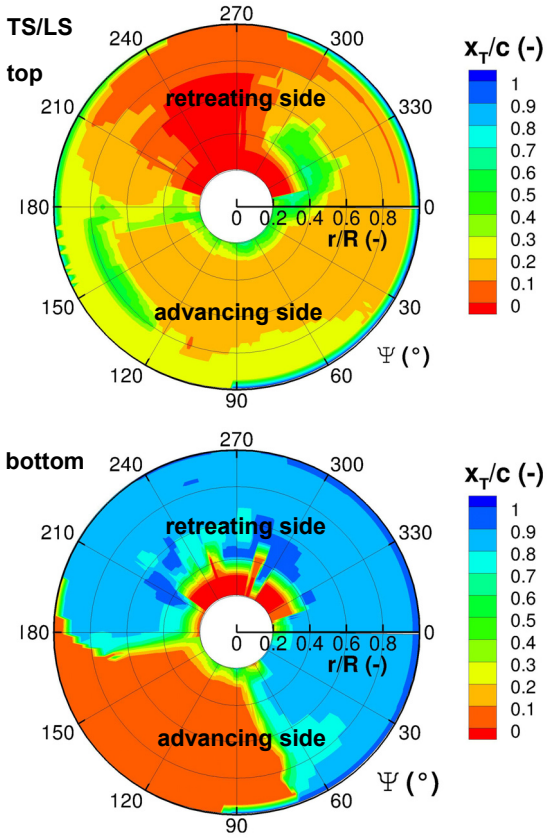

Figure 15: 7AD rotor in forward flight – transition onset over the rotor disk due to pure TS/LS instabilities (AHD criterion, μ=0.33, M=0.2, Re_{TIP}=0.86 mio).

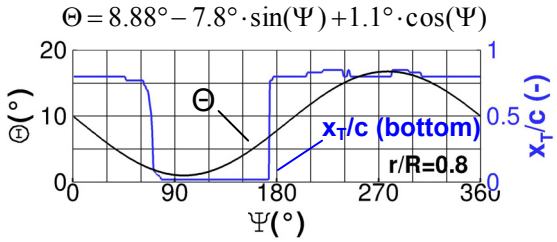

Figure 16: 7AD rotor in forward flight – prescribed pitch angle at the blade root and transition onset (TS/LS) (μ=0.33, M=0.2, Re_{TIP}=0.86 mio, r/R=0.8).

A high pitch, as present on the retreating side of the rotor, leads to high angles of attack. Thus, transition onset shifts towards the LE on the upper side and to the vicinity of the TE on the lower side (see Figure 15, *Ψ=[210°; 270°]*). The high acceleration and deceleration of the flow resulting from the pitch positions seems to overrule the destabilizing effects of the general

high Tu levels in the rotor environment (compare Figure 20). Areas of reverse flow are detected on the retreating side of the rotor at the inner part of the blade (compare Figure 15, *Ψ=[210°; 300°]*, r/R < 0.4).

6.2 Crossflow and attachment line contamination

The transition positions resulting due to pure CF are presented in Figure 17 for a complete rotor revolution. On the upper side of the rotor, CF coincides with high local yaw angles (|Λ| > 30°) (compare Figure 18, *Ψ=[150°; 360°], r/R<0.7*).

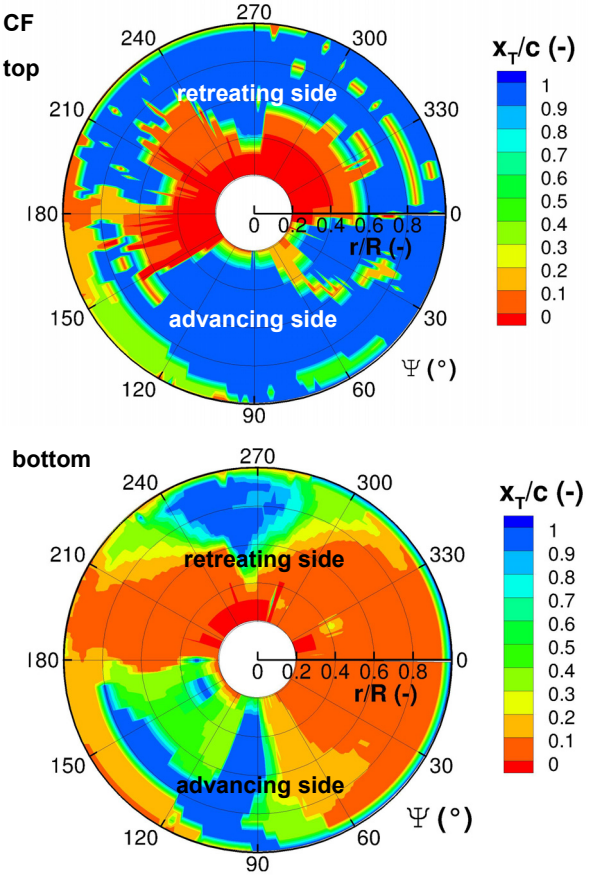

Figure 17: 7AD rotor in forward flight – transition onset over the rotor disk due to pure CF instabilities (C1 criterion, μ=0.33, M=0.2, Re_{TIP}=0.86 mio).

The transition onset occurs at the inner blade part (r/R < 0.7), close to the LE. The sudden transition onset at the LE results from the small region of accelerated flow within the suction peak, where CF can occur. The tip region is also affected by CF when the blade is oriented nearly parallel to the freestream (see Figure 17, top, *Ψ=[150°; 180°]*).

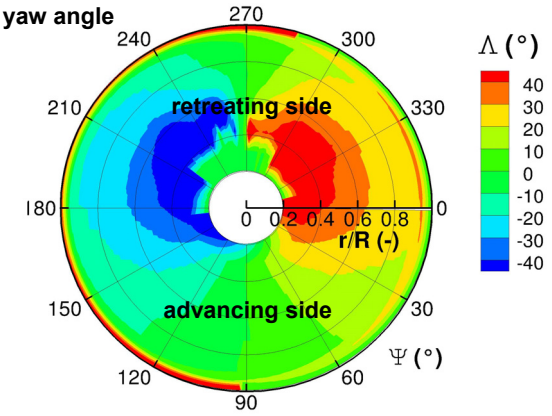

Figure 18: 7AD rotor in forward flight – yaw angle of the incident flow over the rotor disk (μ=0.33, M=0.2, Re_{TIP}=0.86 mio).

Concerning the lower side of the rotor, CF transition occurs over the entire revolution. The onset of CF approximately correlates to a critical yaw angle of |Λ| > 15° (compare Figure 18) for chord Reynolds numbers of up to 2.6 million. The CF limits laminar flow to 5-10% chord length along major parts of the blade lower side. For the present simulation case, ALT did not occur at the blade at any position during the revolution. This can be explained by the small airfoil nose radii, favouring high flow transport out of the stagnation point (dUe/ds, see chapter 3.3.4) – thus preventing contamination effects.

6.3 Bypass transition

Figure 20 shows the local Tu levels encountered by the blades during one revolution. The high Tu levels of up to 15% indicate BVIs on the advancing and retreating side (see Figure 20, *Ψ~90°/270°*). The Byp mechanism (Mayle criterion) strongly reacts to the Tu level within the rotor environment. The predicted Byp transition positions of the rotor generally correlate to the hotspots of high Tu levels (compare Figure 19/Figure 20). On the advancing rotor side, laminar flow is limited to 10% chord length on both upper and lower side (see Figure 19, *Ψ=[80°; 120°], r/R<0.85*).

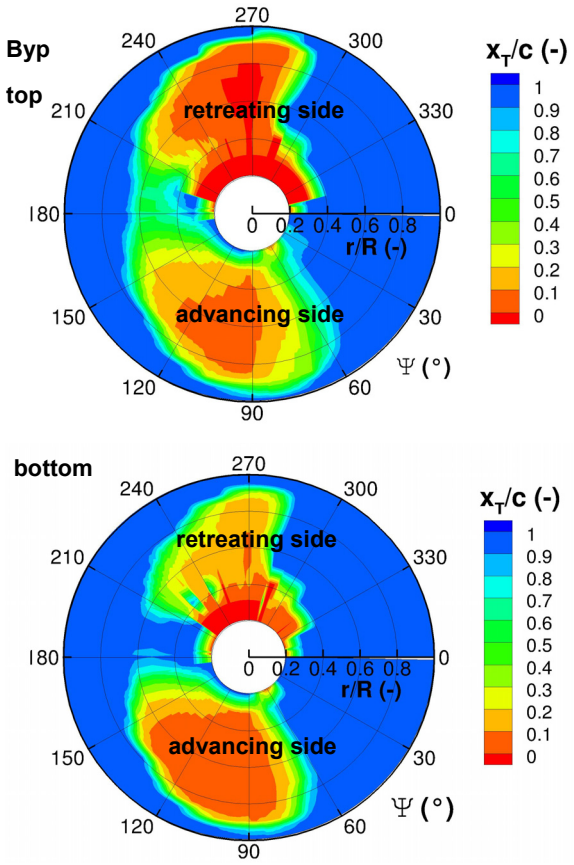

Figure 19: 7AD rotor in forward flight – transition onset over the rotor disk due to pure Byp instabilities (Mayle criterion, μ=0.33, M=0.2, Re_{TIP}=0.86 mio).

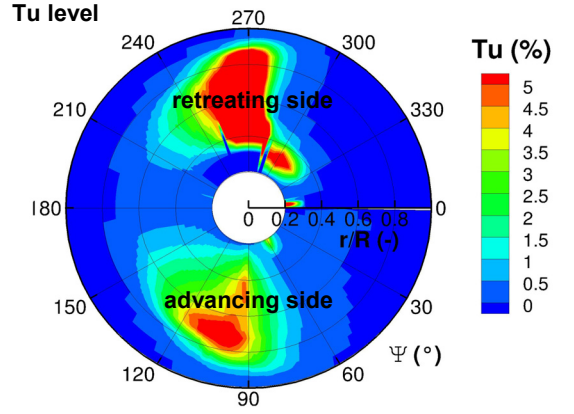

Figure 20: 7AD rotor in forward flight – RANS based Tu level near the leading edge over the rotor disk (μ=0.33, M=0.2, Re_{TIP}=0.86 mio).

The same behaviour can be observed for the retreating side (Figure 19, *Ψ=[210°; 280°]*). Overall, the predicted Byp mechanism behaves plausible but should be related to an eventually unphysical expansion of the rotor wake due to numerical effects.

6.4 Effective laminar flow

For the test case of the 7AD rotor at forward flight, the effective laminar running lengths are presented in Figure 21. The effective transition results from the most upstream transition location of all considered mechanisms, as discussed in chapters 6.1 – 6.3.

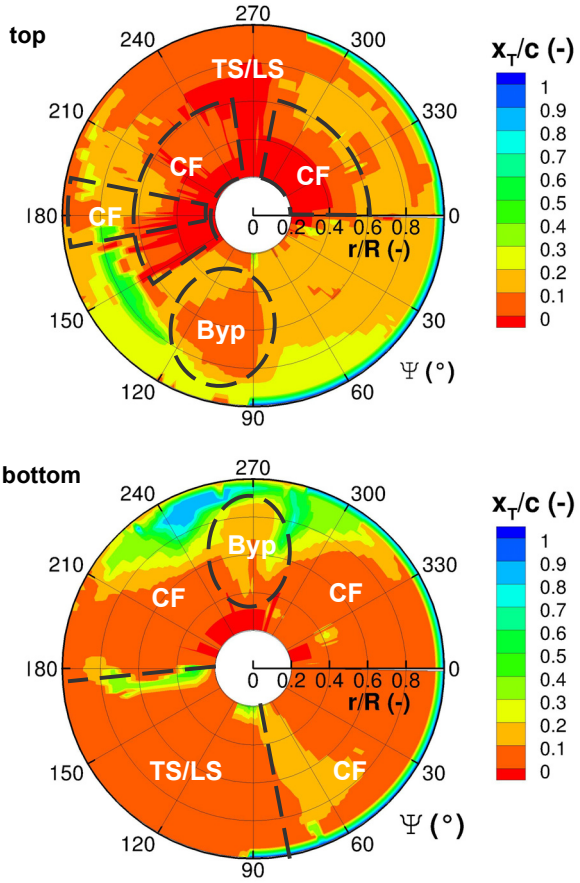

Figure 21: 7AD rotor in forward flight – effective transition mechanism and onset position over the rotor disk (TS/LS, CF, Byp and ALT, μ=0.33, M=0.2, Re_{TIP}=0.86 mio).

On the upper side of the rotor, transition onset is triggered for the most part by TS/LS instabilities due to the adverse pressure gradients in chordwise direction. BVI phenomena and high local yaw angles lead to Byp and CF transition in the second quadrant of the advancing side (see

Figure 21, *Ψ=[90°; 180°]*). On the retreating side, CF transition occurs at the inner part of the blade due to very high local yaw angles of |Λ| > 30° (compare Figure 18). Average laminar running lengths persist for 20% chord length on the advancing side and 8% on the retreating side. On the lower side of the rotor, transition is triggered mainly by CF instabilities. The occurrence of CF transition coincides with high local yaw angles (Figure 18, |Λ|>15°) and the presence of a flat pressure distribution at the lower side of the airfoil. In the second quadrant of the lower advancing side, small and negative angles of attack due to low commanded blade pitch lead to TS/LS transition at the LE. At Ψ~270°, BVI phenomena lead to Byp transition close to the LE. Average laminar running lengths on the lower side exists for 5% chord length on the advancing and 23% on the retreating side.

A comparison of the predicted and the measured BL state is given in Figure 22 and Figure 23 for two radial stations (*r/R=0.6, 0.8*) on the upper side of the blades. The shown experimental data represents the only available transition measurements of the GOAHEAD wind tunnel test. The hotfilm data do not give information about the exact position of transition but about the laminar-turbulent state of the BL at two sensor locations.

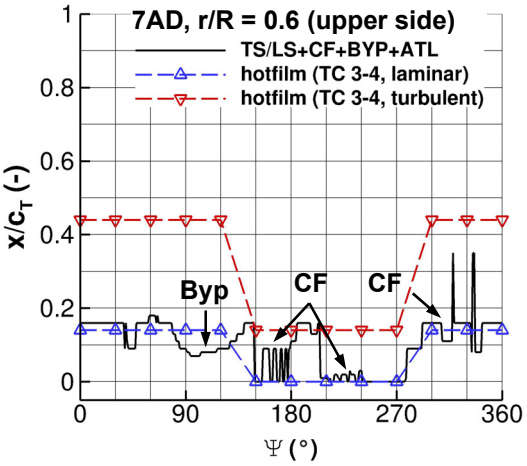

Figure 22: 7AD rotor in forward flight – comparison of measured BL state (hotfilm data [18]) and computed transition onset (μ=0.33, M=0.2, Re_{TIP}=0.86 mio., r/R=0.6).

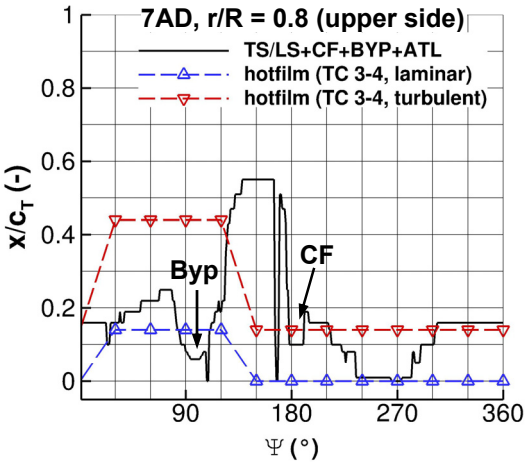

Figure 23: 7AD rotor in forward flight – comparison of measured BL state (hotfilm data [18]) and computed transiton onset (μ=0.33, M=0.2, Re_{TIP}=0.86 mio., r/R=0.8).

The laminar state of the BL is resonably well predicted on the upper side at *r/R=0.6* for one revolution (see Figure 22). The influence of Byp transition at *Ψ=120°* is not present in the experimental data. For the measurements at *r/R=0.8* the agreement is fair (see Figure 23). A large difference in the predicted and measured BL state can be observed for *Ψ=150°*. For both deviations at *Ψ=120°, 150°* rotor trim and blade elasticiy could be relevant and remain to be studied further.

6.5 Influence of laminar flow on required rotor power

In order to study the effect of TS, CF, Byp, and ALT transition on the required rotor power, four cases with transition prediction are investigated (see Table 1). The resulting rotor coefficients (c_P, c_T) are averaged over one revolution and normalized using fully turbulent results (see Figure 24). In the case of pure TS/LS mechanisms, the power coefficient differs by -5% to a fully turbulent calculation (see Figure 24). The average predicted laminar flow on the upper and lower side of the blades exists over 17% and 59% chord length (see Table 1). If in addtion CF transition is taken into account, the difference to the fully turbulent c_P value is -2.4% due to shorter laminar flow on the upper side (x/c_T=15%) and especially on the lower side (x/c_T=19%) (compare Table 1). If Byp transition

is considered, the required rotor power differs by -2% to the fully turbulent computations. Average laminar flow extends over 14% chord length on both upper and lower side of the blades. Since AL contamination does not occur for the present test case, the coefficients remain unchanged. The difference of -2% in required rotor power between a fully turbulent and laminar-turbulent calculation is in principle comparable to the findings of Beaumier and Houdeville [3], which studied drag prediction for a 7A rotor in forward flight, respecting TS/LS and CF transition, using a full potential/BL-code combination.

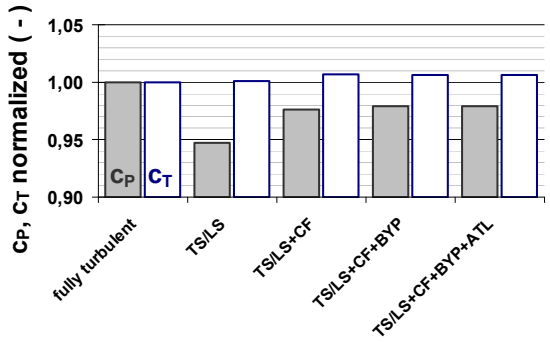

Figure 24: 7AD rotor in forward flight – comparison of rotor coefficients for laminar-turbulent calculations (values related to fully turbulent results, μ=0.33, M=0.2, Re_{TIP}=0.86 mio).

Transition mechanisms	x_T/c (top)	x_T/c (bottom)
TS/LS	0.17	0.59
TS/LS+CF	0.15	0.19
TS/LS+CF+BYP	0.14	0.14
TS/LS+CF+BYP+ALT	0.14	0.14

Note: laminar flow lengths averaged for r/R>0.7 during one rotor revolution

Table 1: 7AD rotor in forward flight –cases of laminar-turbulent computations and average laminar running lengths.

7. CONCLUSION

The laminar-turbulent flow transition on helicopter rotors in hover and forward flight was investigated using the block structured RANS solver FLOWer of DLR. The investigation employed empirical criteria and covered transition due to TS and CF instabilities, laminar separation, Byp and AL contamination. The streamwise laminar BL quantities were calculated based on the assumption of an infinite swept wing by an integral method. A set of chord- and spanwise velocity profiles provided laminar BL parameters in crossflow direction. The basic validation for the NLF-0416 airfoil under steady flow conditions (*M=0.1, Re=4 million, α=[-4°;12°]*) showed close agreement of the predicted transition onset positions to the experimental data. A hover test case referring to a BO 105 flight test was used to further validate the transition prediction method. The general agreement to the flight test data is close. All investigated transition mechanisms were observed to occur on the rotor blade at hover, except ALT. TS/LS transition dominated the main part of the blade (*r/R=[0.4; 0.8]*). The tip region is heavily affected by Byp transition due to BVI. Nevertheless, the laminar-turbulent calculations gave a +4% higher FM compared to fully turbulent computations. The isolated 7AD rotor at cruise condition (GOAHEAD TC 3-4, *M=0.2, μ=0.33, Re_{TIP}=0.86million*) served as a test case to predict transition on a rotor in forward flight. On the upper side, mainly TS/LS transition occurs due to the strong acceleration and deceleration of the flow. CF occurs at the inner blade parts. The lower side of the rotor is mostly dominated by CF transition, favoured by the high yaw angles and flat pressure distributions. Byp transition due to local BVI at *Ψ~90°/270°* further limits the laminar flow. The predicted rotor power of the laminar-turbulent calculation differs from the fully turbulent value by -2%. If only TS/LS mechanisms are considered the difference is -5%. Comprehensive rotor codes which use 2D airfoil data with TS/LS transition, can consequently underestimate the c_P by -3% due to the neglection of possible Byp and CF transition.

Further studies should cover the influence of mesh refinement, blade elasticity and Reynolds number on the predicted transition positions for helicopter rotors. Additional activities may be directed towards a deeper validation of the employed laminar velocity profiles. The general experimental basis for validation of transition on

helicopter rotors, however, is sparse and should be improved in future research projects.

ACKNOWLEDGEMENTS

This work has been supported and partly funded by EUROCOPTER Deutschland.

REFERENCES

[1] Arnal, D.: “Three-dimensional boundary layers: laminar-turbulent transition”, AGARD Report No 741, Toulouse Cedex, 1987.

[2] Arnal, D., Casalis, G., Houdeville, R.: “Practical Transition Prediction Methods: Subsonic and Transonic Flows”, RTO-AVT/VKI Lecture Series, RTO-EN-AVT-151, 09-12 June, Rhode St. Genèse, Belgium, 2008.

[3] Beaumier P., Houdeville, R.: ”3D laminar-turbulent boundary layer calculations on helicopter rotors in forward flight: application to drag prediction.”, ONERA Technical Paper, TP 1995-103, Chatillon Cedex, 1995.

[4] Blaser, D. A., Velkoff, H. R.: „A Preliminary Analytical and Experimental Investigation of Helicopter Rotor Boundary Layers“, AIAA Journal, Vol. 11, No. 12, pp.1660-1664, 1973.

[5] Depommier, G., Alfano D., Leusink, D. and Leymary, G.: “Computation of Transition to Turbulence on Rotor Blades”, 37th ERF 2011, 13.-15. Sept., Milano, Italy, 2011.

[6] Dietz, M., Schimke, D.: „Gesamthubschrauber-simulation durch CFD: Entscheidende Schritte auf dem Weg zur Realisierung“, DGLR Kongress, Hamburg, Germany, 2010.

[7] Dwyer, H.A., McCroskey, W.J.: „Crossflow and Unsteady Boundary-Layer Effects on Rotating Blades“, AIAA Jounal, Vol. 9, No. 8, pp.1408-1505, 1971.

[8] Heister, C. C., Raddatz, J. and Klein, A.: “ *Accurate Numerical Flow Simulation of Hovering Rotors using different Transition Prediction Methods”,* 36th ERF 2010, 06.-09.Sep., Paris, France, 2010.

[9] Heister, C. C.: “Semi-/empirical transition prediction and application to an isolated rotor in hover.” International Journal of Engineering Systems Modelling and Simulation, 4 (1/2), pp. 69-78. Inderscience Enterprises Ltd. ISSN 1755-9758, 2012.

[10] Hill, J.L., Shaw, S.T. and Qin, N.: “Engineering prediction of laminar/turbulent transition for isolated helicopter rotors in hover”, RaeS Aerospace Aerodynamics Resource Conference, London, UK, 2004.

[11] Leishman, J.G.: „Principles of Helicopter Aerodynamics“, Cambridge University press, 2nd edition, New York, 2006.

[12] Mayle, R.E.: “The Role of Laminar-Turbulent Transition in Gas Turbine Engines”, ASME Journal of Turbomachinery, Vol.113, pp.509-537, Oct. 1991.

[13] Poll, D.I.A.: ”Some aspects of the flow near a swept attachment line with particular reference to boundary layer transition”, Cranfield Institute of Technology, Co A Report No. 7805, 1978.

[14] Raddatz, J., Fassbender, J.: “Block Structured Navier-Stokes Solver FLOWer”, *MEGAFLOW – Numerical Flow Simulation for Aircraft Design*, edited by N. Kroll and J. Fassbender, Vol. 89 of *Notes on Numerical Fluid Mechanics and Multidisciplinary Design*, Springer Verlag, 2005.

[15] Rohardt, C.H.: “Flow Visualization on a Helicopter Rotor in Hover Using Acenaphthen”, 13th European Rotorcraft Forum, Arles, France, 1987.

[16] Schlichting, H., Gersten, K.: “Grenzschicht-Theorie”, Springer Verlag Berlin Heidelberg, ISBN-10 3-540-23004-1, 10. Auflage, 2006.

[17] Schwarz, Th., Pahlke, K.: “CFD code validation for complete helicopters – The European GOAHEAD project”, American Helicopter Society 67th Annual Forum, 3.-5. Mai 2011, Virginia Beach, VA, USA, 2011.

[18] Séraudie, A.: “Blade hot film results and delivery to the database”, Report GOAHEAD / WP3 / ONERA / D3.8.3, CN AST4-CT-2005-516074, 2008.

[19] Somers, D.A.: “Design and experimental results for a natural laminar flow airfoil for general aviation applications”, NASA Technical Paper 1861, Scientific and technical information branch, 1981.

[20] Walz, A.: „Strömungs- und Temperatur-grenzschichten“, Verlag G. Braun, Best.-Nr. 4241, Karlsruhe, 1966.

[21] Zografakis, G. Barakos, G., Johnson M.: “Transition Modelling for Rotorcraft CFD“, 34th ERF 2008, 16.-19. Sept., Liverpool, UK, 2008.